Accepted Manuscript

Correlation between crystallographic and microstructural features and low hysteresis behavior in $Ni_{50.0}Mn_{35.25}In_{14.75}$ melt-spun ribbons

Haile Yan, C.F. Sánchez-Valdés, Yudong Zhang, J.L. Sánchez Llamazares, Zongbin Li, Bo Yang, Claude Esling, Xiang Zhao, Liang Zuo

PII: S0925-8388(18)32564-7

DOI: 10.1016/j.jallcom.2018.07.063

Reference: JALCOM 46779

To appear in: *Journal of Alloys and Compounds*

Received Date: 27 November 2017

Revised Date: 11 June 2018

Accepted Date: 7 July 2018

Please cite this article as: H. Yan, C.F. Sánchez-Valdés, Y. Zhang, J.L. Sánchez Llamazares, Z. Li, B. Yang, C. Esling, X. Zhao, L. Zuo, Correlation between crystallographic and microstructural features and low hysteresis behavior in $Ni_{50.0}Mn_{35.25}In_{14.75}$ melt-spun ribbons, *Journal of Alloys and Compounds* (2018), doi: 10.1016/j.jallcom.2018.07.063.

Correlation between crystallographic and microstructural features and low hysteresis behavior in $Ni_{50.0}Mn_{35.25}In_{14.75}$ melt-spun ribbons

Haile Yan[1, *], C. F. Sánchez-Valdés[2], Yudong Zhang[3,4], J. L. Sánchez Llamazares[5, **], Zongbin Li[1], Bo Yang[1, 6], Claude Esling[3,4], Xiang Zhao[1], Liang Zuo[1]

[1]*Key Laboratory for Anisotropy and Texture of Materials (Ministry of Education), School of Material Science and Engineering, Northeastern University, Shenyang 110819, China.*
[2]*División Multidisciplinaria, Ciudad Universitaria, Universidad Autónoma de Ciudad Juárez (UACJ), calle José de Jesús Macías Delgado # 18100, Ciudad Juarez, Chihuahua, México.*
[3]*Laboratoire d'Étude des Microstructures et de Mécanique des Matériaux (LEM3), CNRS UMR 7239, Université de Lorraine, 57045 Metz, France.*
[4]*Laboratory of Excellence on Design of Alloy Metals for low-mAss Structures (DAMAS), Université de Lorraine, 57045 Metz, France.*
[5]*Instituto Potosino de Investigación Científica y Tecnológica, Camino a la Presa San José 2055, Col. Lomas 4ª, San Luis Potosí, S.L.P. 78216, Mexico.*
[6] *Northeastern Institute of Metal Materials Co., Ltd, Shenyang 110108, China*

Abstract. In this work, crystallographic, microstructural and magnetocaloric investigations were performed on textured $Ni_{50}Mn_{35.25}In_{14.75}$ melt-spun ribbons with low thermal (6 K) and magnetic-field induced hysteresis (–0.73 $J \cdot kg^{-1}$ at 2 T) and moderate maximum magnetic entropy change ΔS_M^{max} (11 $J \cdot kg^{-1} \cdot K^{-1}$ at 5T) at room temperature (302 K). The austenite in the ribbons crystallizes into a $L2_1$ structure, whereas martensite has a monoclinic incommensurate 6M modulated structure as determined with the superspace theory. By means of electron backscatter diffraction technique, the morphological and crystallographic features of microstructure were systematically characterized. Ribbons possess a fine microstructure with an average grain size (initial austenite phase) of around 10 μm, whereas the 6M martensite has a self-accommodated microstructure with 4 kinds of twin-related martensite variants. During inverse martensitic transformation, the austenite prefers to nucleate at the grain boundaries of initial austenite. By means of cofactor conditions and crystallographic orientation analyses, the good geometrical compatibility between austenite and martensite was confirmed. Based on the crystal structure and microstructure information obtained, the reason of the low thermal hysteresis was discussed.

Keywords: Ni–Mn–In; ribbon; martensitic transformation; electron backscatter diffraction; hysteresis; magnetocaloric effect.

[*]Corresponding author. Dr. Haile Yan
Key Laboratory for Anisotropy and Texture of Materials (Ministry of Education), School of Material Science and Engineering, Northeastern University, Shenyang 110819, China.
Tel: +86-24-83681723, E-mail address: yanhaile@mail.neu.edu.cn

[**]Corresponding author. Dr. José Luis Sánchez Llamazares
Instituto Potosino de Investigación Científica y Tecnológica A.C., Camino a la Presa San José 2055, Col. Lomas 4ª sección, San Luis Potosí, S.L.P. 78216, México
Tel: +52-444-8342000. E-mail address: jose.sanchez@ipicyt.edu.mx

1. INTRODUCTION

In the last decade, Heusler-type Ni–Mn–X based alloys (X = In, Sn and Sb) have been extensively studied owing to their giant and tunable first-order magnetocaloric effect (MCE) near room temperature. The latter makes them promising materials for their utilization as active magnetic regenerators in solid-state magnetic refrigeration devices [1-14]. The giant MCE of these materials originates when the first-order magneto-structural transition occurs from a weak-magnetic martensite to a ferromagnetic austenite [15-22]. Unfortunately, both thermal hysteresis ΔT_{hyst} and magnetic field-induced hysteresis intrinsically associated with the magneto-structural transition are the two relevant phenomena that hinders their potential use, since these hystereses would reduce the refrigeration capacity and further result in the degradation of the properties after several cycles [16, 23, 24]. Therefore, the understanding of physical mechanisms to reduce the hysteresis loss across magneto-structural transition are crucial for the designing and fabrication of low-hysteresis Ni–Mn–X based alloys as key points towards their utilization in practical refrigeration devices.

In the framework of thermodynamics, the *Gibbs* free energies of the parent and the product phases are equal at the thermodynamic equilibrium state. Thus, the driving force of magneto-structural transition vanishes. Thermal or magnetic hysteresis may occur since the transformation driving force should be large enough to overcome the phase transformation energy barriers or resistances [24-27]. Thus, in theory, two routes would be effective to decrease the hysteresis losses associated to the magneto-structural transition. One is reducing the resistance of magneto-structural transition. In such a sense, the decrease of the geometrical incompatibility between the parent and the product phases has been the most successful case [6, 23, 28]. In fact, following this approach several low thermal hysteresis Heusler-type bulk alloys, such as $Ni_{50.4}Mn_{34.8}In_{15.8}$ (8 K) [6], $Ni_{51}Mn_{33.4}In_{15.6}$ (4 K) [29], and $Ni_{45}Co_5Mn_{40}Sn_{10}$ (6 K) [30] have been reported. The other is to promote the progress of magneto-structural transition by tuning the phase/microstructure constituent [31-33]. Very recently, *T. Gottschall* et. al [34, 35] found that a minor loop at the middle temperature region of the magneto-structural transition could significantly reduce the hysteresis loss, since it is not necessary to nucleate new phase during structural transition and then the required energy is reduced. Besides, introducing appropriate crystal defects, such as grain boundaries, as nucleation sites could be also an alternative method to promote the structural transition.

The melt-spinning technique, characterized by an ultra-rapid cooling and solidification process, has been developed to be an effective method for the preparation of single-phase Heusler-type Ni–Mn–X alloy ribbons with crystallographic preferred orientation (texture) [36-39]. In this work, textured $Ni_{50}Mn_{35.25}In_{14.75}$ ribbons with a low thermal and magnetic hysteresis loss accompanying with magneto-structural transition were fabricated by melt-spinning technique and no special effort, such as heat treatment, was made to develop its microstructure or atomic order degree. The crystal structure, the morphological and crystallographic features of microstructure and magnetic properties of these ribbons were examined by means of X-ray diffraction (XRD), electron backscattering diffraction (EBSD) and magnetization measurements. The origin of the low thermal hysteresis observed is discussed in terms of the geometrical compatibility between austenite and martensite, and the morphological and crystallographic microstructural features. This study could shed some light on the performance optimization to decrease the hysteresis loss associated with the first-order magneto-structural transformation.

2. **EXPERIMENTAL DETAILS**

A bulk master alloy with nominal composition $Ni_{50}Mn_{35.25}In_{14.75}$ was prepared by arc-melting pure Ni (99.97 wt.%), Mn (99.95 wt.%) and In (99.995 wt.%) elements. Due to the high vapor pressure of Mn, 1% extra Mn was added to compensate the weight loss. The sample was then thermally annealed at 1173 K for 24 h to enhance the composition homogeneity and the degree of atomic order. The melt-spun ribbons were fabricated by using a single copper roller at a wheel rotating speed of 15 m/s to obtain a good shape and strong crystallographic preferred orientation [40, 41]. The actual composition of ribbons was determined to be $Ni_{49.3}Mn_{35.7}In_{15.0}$ by energy dispersive spectroscopy (EDS), which is similar to the nominal one.

The crystal structure of ribbons was examined by means of X-ray diffraction with *Cu-Kα* radiation (λ=1.5418Å) using a Rigaku Smartlab X-ray diffractometer equipped with a graphite monochromator at room temperature. The microstructural investigations were performed in a field emission gun scanning electron microscope (SEM, Jeol JSM 6500 F) with both back-scattered electron (BSE) and electron backscatter diffraction (EBSD) detectors. To avoid stress-induced effects on martensitic transformation, no mechanical surface ground or polishing of ribbons was carried out. Instead, the ribbon surfaces were directly electrolytically polished at 263 K with a 20 % nitric acid solution in methanol under a voltage of 8 V. The texture of austenite

and martensite of ribbons was investigated using a Rigaku Smartlab X-ray diffractometer and Mtex software package [42]. Magnetization measurements were carried out in a Quantum Design physical property measuring system (PPMS-9T) Evercool-I equipped with the vibrating sample magnetometer module. The magnetic field was applied along the ribbon length direction (rolling direction) on a parallelepiped-shaped sample (of physical dimensions: 20 μm in thickness, 0.5 mm in width and 3 mm in length, cut from the central region of a ribbon), to minimize the effect of the internal demagnetizing field

3. **RESULTS AND DISCUSSION**

Figs. 1(a) and (b) show the temperature dependence of magnetization (M-T curve) of $Ni_{50}Mn_{35.25}In_{14.75}$ melt-spun ribbons under static magnetic fields of 5 mT, and 1 T and 5 T, respectively. The curves were recorded at a temperature sweep rate of 1.0 $Kmin^{-1}$. From the low-field *M-T* curve (5 mT), the first-order magneto-structural transition from a ferromagnetic austenite to a weak-magnetic martensite is observed around room temperature. The splitting between ZFC and FC (FH) curves below the Curie temperatures of martensite (T_C^M= 132 K) indicates the coexistence of the ferromagnetic and antiferromagnetic couplings in the martensite state [43, 44]. As shown in Fig. 1(b), as the applied magnetic field increases from 1 T to 5 T, the temperatures of the magneto-structural transition decrease. The temperatures of forward (T_M) and inverse (T_A) magneto-structural transition and the Curie temperatures of austenite (T_C^M= 132 K) and martensite (T_C^A = 307 K) under different magnetic fields, estimated from the d*M*/d*T* vs. *T* curve, are summarized in Table 1. The magnetic field dependence of T_M and ΔT_{hys} (estimated as $\Delta T_{hys} = T_A - T_M$) is given in Fig. 1(c). A linear relationship between the T_M and the applied magnetic field is observed with a slope of –2 K/T, suggesting that a magnetic-field-induced inverse martensite transformation could happen when the external magnetic field is applied under certain temperature. Note that the magneto-structural transition of the studied melt-spun ribbons exhibits a thermal hysteresis as low as 6 K, which is very small compared with the one typically found in conventional NiMnIn-based alloys, such as $Ni_{50.4}Mn_{34.9}In_{14.7}$ (10 K) [37], $Ni_{45.5}Co_{4.5}Mn_{36.6}In_{13.4}$ (15 K) [45], $Mn_{50}Ni_{40}In_{10}$ (38 K) [46] and $Ni_{45}Co_5Mn_{36.8}In_{13.2}$ (30 K) [47] alloy. As the applied magnetic field increases to 1 T and 5 T, ΔT_{hys} increases to 8 K and 10 K, respectively. The similar magnetic field dependence of ΔT_{hys} has also been observed in $Ni_{45.7}Mn_{36.6}In_{13.5}Co_{4.2}$ [48] and $Ni_{52}Co_7Mn_{25}In_{16}$ [49] alloys.

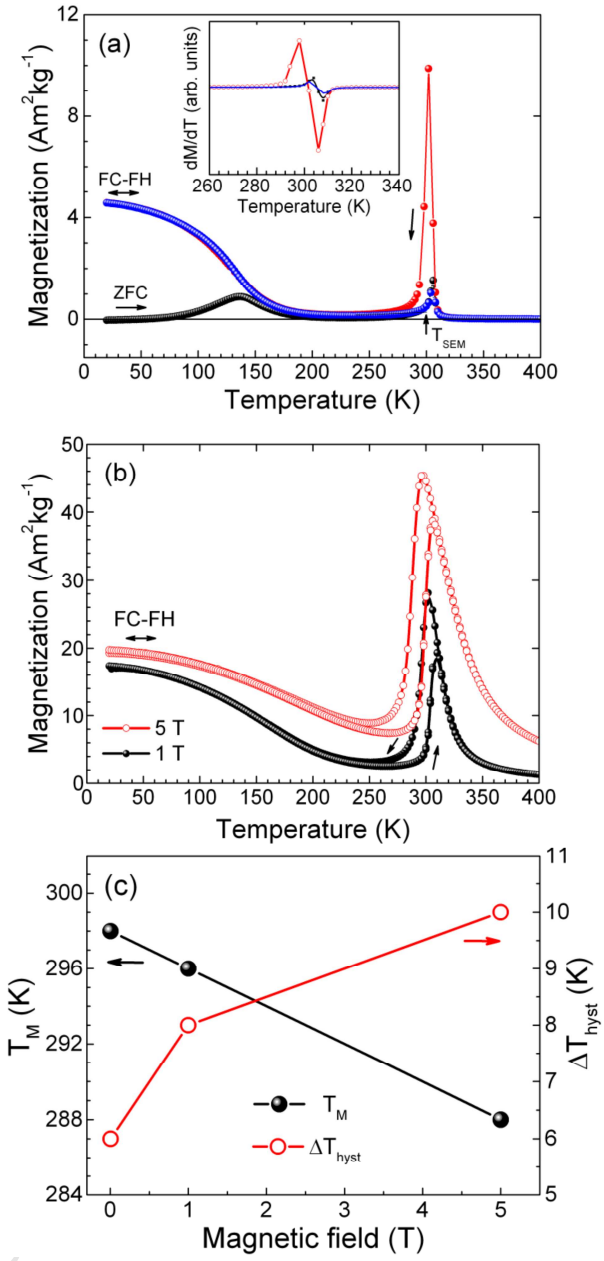

Fig. 1 *M*-*T* curves of melt-spun $Ni_{50}Mn_{35.25}In_{14.75}$ ribbons under applied magnetic fields of 5 mT (a), and 1 T and 5 T (b), following zero-field cooled (ZFC), field-cooled (FC) and field heating (FH) protocols. d*M*/d*T* vs. *T* plot under μ_oH = 5 mT is inserted in (a). The temperatures of the forward martensitic transformation and the thermal hysteresis of the magneto-structural transition (ΔT_{hys}) as a function of the applied magnetic field is given in (c). T_{SEM} in (a) is the temperature at which SEM/EBSD measurements were performed to indicate the sample history of heat treatment.

Table 1 Temperatures of the forward (T_M) and the inverse (T_A) martensitic transformation and thermal hysteresis of magneto-structural transition (ΔT_{hys}) under the magnetic fields of 5 mT, 1 T and 5 T, and Curie temperatures of austenite (T_C^A) and martensite (T_C^M) for $Ni_{50}Mn_{35.25}In_{14.75}$ melt-spun ribbons.

$\mu_o H$ (T)	T_M (K)	T_A (K)	ΔT_{hys} (K)	T_C^A (K)	T_C^M (K)
0.005	298	304	6	307	132
1	296	304	8	–	–
5	288	298	10	–	–

Fig. 2(a) shows isothermal magnetization curves measured up to a maximum magnetic field of 5 T with a temperature step of 1 K across the magneto-structural transition. A thermal protocol with a thermal cycling at zero magnetic field from 400 K to 200 K to the measuring temperature T_{meas} was performed prior to recording each isothermal magnetization curve. As shown in Fig. 2(a), the ribbons exhibit a typical paramagnetic behavior below 290 K revealed by the nearly linear field dependence of magnetization. Above 290 K, a magnetic-field-induced metamagnetic transition is observed. The S-shape trend of the Arrott plots, shown at the inset of Fig. 2(a), confirm the first-order nature of the metamagnetic transition [50]. Above 307 K, the magnetization of the ribbons decrease with the increase of temperature owing to the second-order Curie transition of austenite. Fig. 2(b) displays the temperature dependence of magnetic entropy change ΔS_M estimated from the isothermal magnetization curves using the *Maxwell* relation [16, 51]. As shown in Fig. 2(b), the smooth first-order magneto-structural transition leads to a moderate positive magnetic entropy change peak of ΔS_M^{max} = 11 $J \cdot kg^{-1} \cdot K^{-1}$ just at room temperature (302 K) under a magnetic field change $\mu_o \Delta H$ of 5 T. The ΔS_M^{max} in the studied ribbons is comparable to the melt-spun ribbons of $Gd_{65}Mn_{25}Ge_{10}$ (4.5 $J \cdot kg^{-1} \cdot K^{-1}$ at 5T) [52], $Ni_{52}Mn_{26}Ga_{22}$ (–11.4 $J \cdot kg^{-1} \cdot K^{-1}$ at 5T) [40] and $LaFe_{11}Co_{0.8}Si_{1.2}$ (13.5 $J \cdot kg^{-1} \cdot K^{-1}$ at 5T) [53] alloys. Above 307 K, the ribbons exhibit a broad negative magnetic entropy change curve, owing to the second-order ferromagnetic transition of austenite [51, 54].

Fig. 2(c) presents the field-up and field-down isothermal magnetization curves across the magnetostructural transition with a maximum field of 2T. Notice that the magneto-structural transition has a quite small magnetic hysteresis loss (as the small areas enclosed between the

field-up and field-down magnetization curves denote). The temperature dependence of magnetic hysteresis losses under the magnetic field of 2 T is shown in Fig. 2(d). A negligible magnetic hysteresis loss with a maximum of –0.73 $J \cdot kg^{-1}$ across the magneto-structural transition is obtained, which is much smaller than that generally observed in Heusler-type refrigerants, such as $Ni_{50}Mn_{18}Cu_7Ga_{25}$ (19.0 $J \cdot kg^{-1}$ at 2 T) [55] and $Ni_{45}Co_5Mn_{36.8}In_{13.2}$ (–96.5 $J \cdot kg^{-1}$ at 2 T) [47]. The total and effective refrigerant capacities under the magnetic field of 2 T are 11.40 $J \cdot kg^{-1}$ and 10.80 $J \cdot kg^{-1}$, respectively.

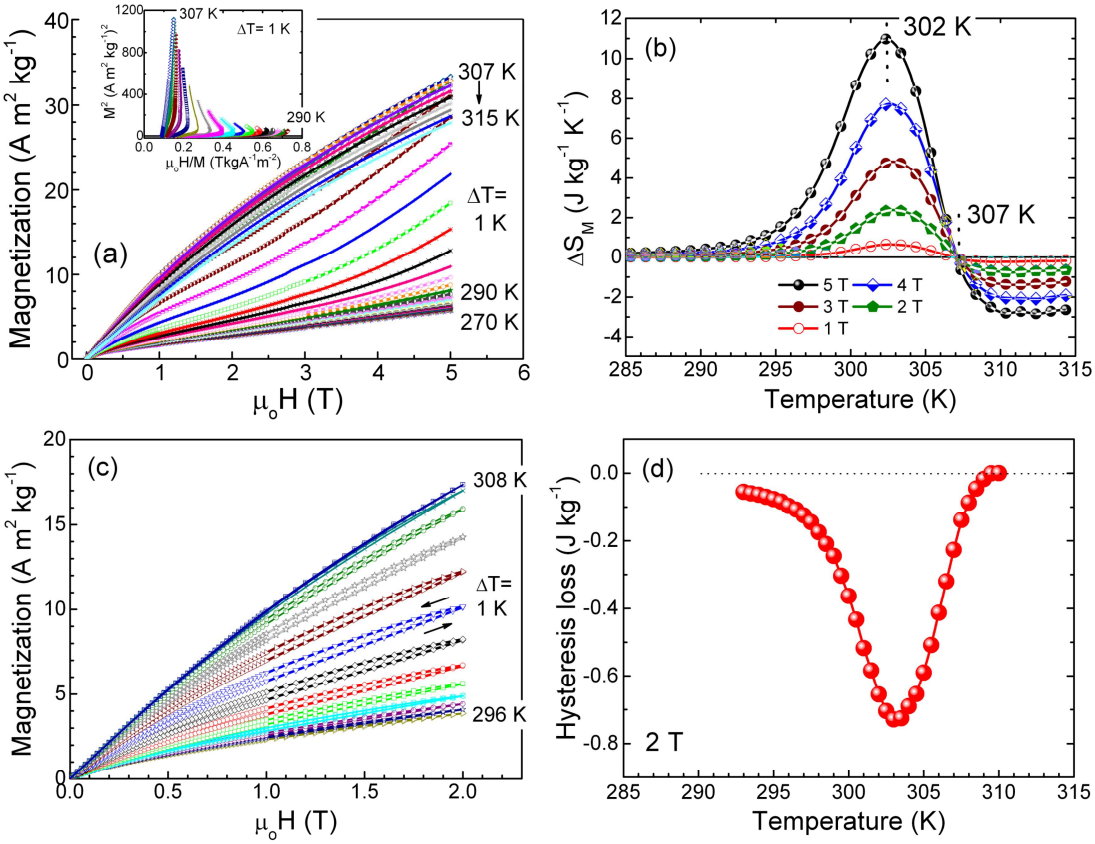

Fig. 2 Set of isothermal magnetization curves up to 5 T (a), Arrott plots (M^2 vs. μ_oH/M) (inset), temperature dependence of magnetic entropy change ΔS_M through the inverse martensitic transformation (b), field-up and field-down isothermal magnetization curves up to 2 T (c), and magnetic hysteresis loss as a function of temperature (d) for $Ni_{50}Mn_{35.25}In_{14.75}$ melt-spun ribbons.

Fig. 3 shows the room temperature X-ray diffraction pattern of the studied melt-spun ribbons. In agreement with the low-field $M(T)$ curve, a mixture of both austenite and martensite

phases coexists in the ribbons at room temperature. For austenite, the presence of the superlattice reflections $(111)_A$, $(113)_A$ and $(331)_A$, indicated in green in Fig. 3, shows that it has a cubic $L2_1$ ($Fm\bar{3}m$) rather than a B_2 ($Pm\bar{3}m$) crystal structure [56, 57]. The lattice parameter is determined to be 6.0010(8) Å. In case of the martensite, the presence of the so-called "satellite reflections" (indicated in blue in Fig. 3) denotes that it has a modulated crystal structure. By means of Le Bail full profile fitting approach [58] and the (3+1)-dimensional superspace theory [59], we found that the martensite has an incommensurate monoclinic 6M modulated structure with superspace group of *I2/m*(*α*0*γ*)*00* [56], and lattice parameters a = 4.3757(4) Å, b = 5.6462(1) Å, c = 4.3227(2) Å and β = 92.506(4)°. The refined structural modulation wave vector, representing the periodicity of structural modulation [59], was $\boldsymbol{q}$ = 0.3506(4) $\boldsymbol{c}^*$. The difference between the measured and simulated patterns is mainly attributed to the crystal defects and residual stresses in melt-spun ribbons. A similar 6M modulated structure (sometimes also labelled as 3M), has recently been reported in $Ni_{50}Mn_{34}In_{14}$ [56] and $Ni_{50}Mn_{35}In_{15}$ [60] alloys.

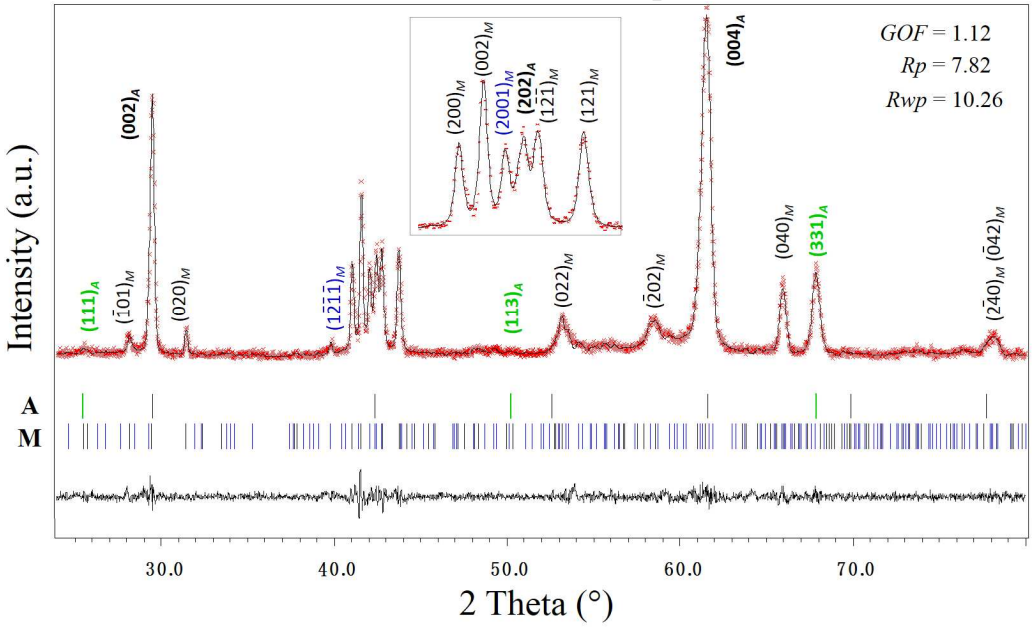

Fig. 3 Experimental (red points) and simulated (black lines) room temperature X-ray diffraction patterns of $Ni_{50}Mn_{35.25}In_{14.75}$ melt-spun ribbons. "*A*" and "*M*" indicate the austenite and the martensite reflections, respectively. Superlattice reflections of austenite and satellite reflections of martensite (generated by the periodic modulation of atomic positions) are indicated in green and blue, respectively. Miller indices of the modulated martensite are labelled in the frame of the (3+1)-dimensional space. Inset: zoom into the 2θ angle interval $40.5 \leq 2\theta \leq 45.0$.

Fig. 4 shows a typical SEM image of the cross-section of $Ni_{50}Mn_{35.25}In_{14.75}$ melt-spun ribbons. It is seen that the thickness of ribbons is around 45 ~ 55 μm. Ribbons are mainly composed of columnar grains with their long axis tending to align perpendicular to ribbon surface. Small equiaxed grains are formed in some localized regions of ribbon surface on the wheel side. The similar microstructures have also been reported in melt-spun ribbons of other Ni-Mn-based alloys [36, 37]. By means of EDS technique, ribbons were confirmed to have a homogeneous chemical composition.

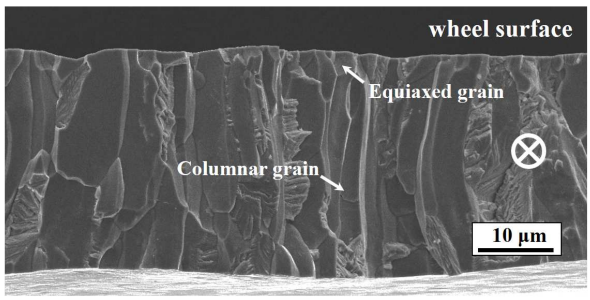

Fig. 4 SEM micrograph of fractured cross-section of $Ni_{50}Mn_{35.25}In_{14.75}$ melt-spun ribbons. The crossed circle symbol indicates the spinning direction.

Fig. 5(a) displays a typical BSE image of the studied melt-spun ribbons taken on their free surface. During the sample preparation, the studied ribbons were electrolytically polished at 263 K, *i.e.*, below the temperature of martensitic transformation (298 K), and then heated to room temperature for microstructural investigations. As the temperature of microstructure investigation T_{SEM} is close to the start temperature of the inverse martensitic transformation, as shown in Fig. 1(a), the microstructure observed in this work represents the early stage of the inverse martensitic transformation. As Fig. 5(a) shows, the specimen is composed by fine elongated zones outlined by the dark boundaries, inherited from initial austenite grains, with a width of about 10 μm. Generally, the homogeneous contrast and plate-shaped morphology zones would represent the newly transformed austenite and 6M martensite, respectively.

Fig. 5(b) shows a typical SEM/EBSD crystallographic orientation micrograph. Notice that austenite, indicated in red color, is primarily located either along the grain boundary regions of the initial austenite or sometimes between martensite plates, suggesting that during the inverse martensitic transformation the austenite phase prefers the grain boundary regions to nucleate. In general, the boundary regions of microstructure favor the nucleation of the new phase, since they

are of large atom spacing, large lattice distortion and high energy. As for martensite, it has a typical self-accommodated microstructure with four orientation variants (A, B, C and D) in one martensite colony, as highlighted in the zoomed white box I in Fig. 5(b). Based on misorientation examinations, all variant pairs were found to be twin-related, and their twin relations are classified into three types, *i.e.* type-I (A: C and B: D), type-II (A: B and C: D) and compound (A: D and B: C) twin [61, 62]. Moreover, as shown in the white box II in Fig. 5(b), it is seen that the austenite is connected by single martensite variants rather than the generally observed "sandwich-like" structures of martensite at the boundaries between austenite and martensite (*habit plane*) [25, 63].

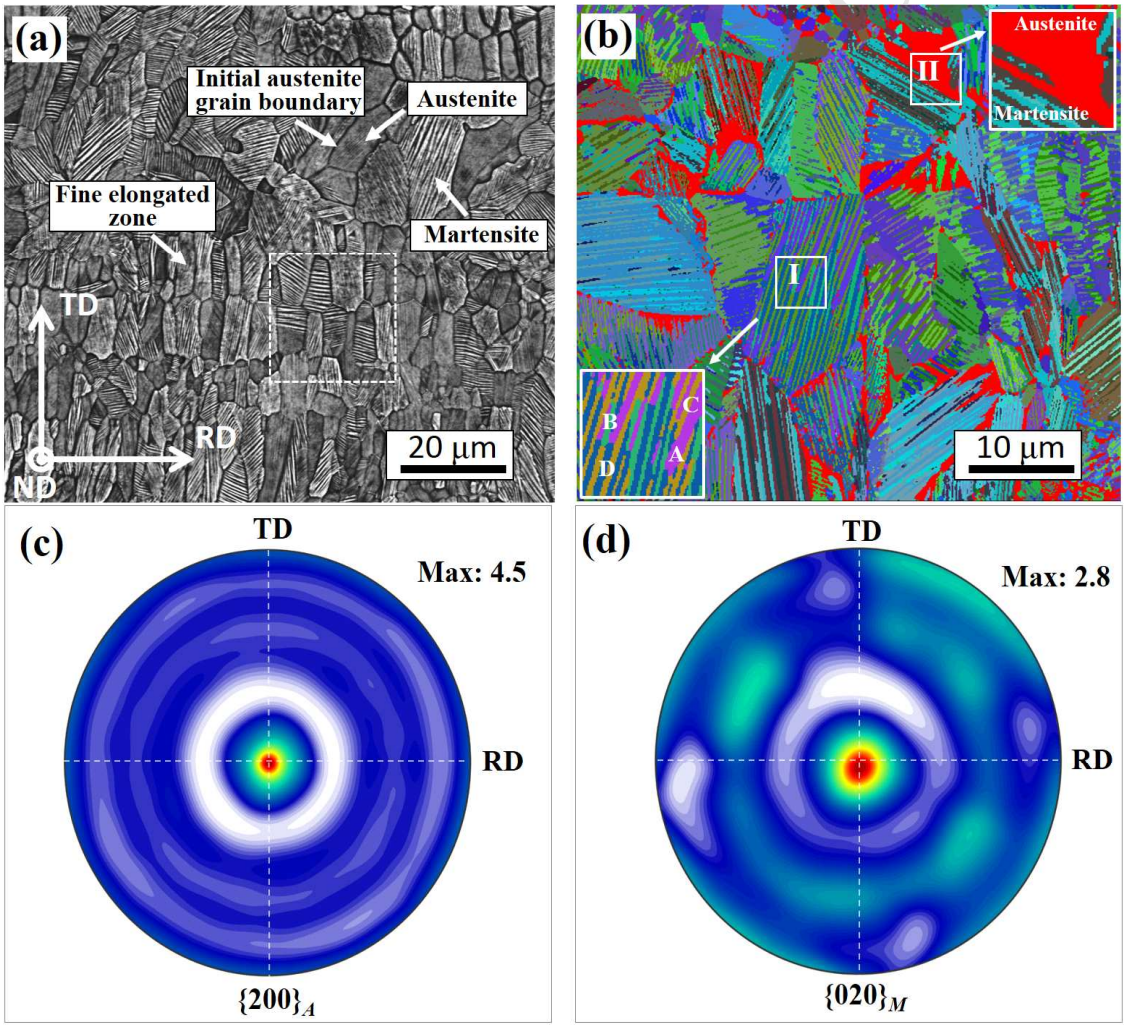

Fig. 5 SEM-BSE micrograph (a), EBSD crystal orientation micrograph (b), $\{200\}_A$ pole figure of austenite (c), and $\{020\}_M$ pole figure of martensite (d), for $Ni_{50}Mn_{35.25}In_{14.75}$ melt-spun ribbons. The martensite is self-accommodated with four orientation variants A, B, C and D.

Figs. 5(c) and (d) display, respectively, the pole figures for austenite ($\{200\}_A$) and the 6M martensite ($\{020\}_M$) measured on the free surface of the studied ribbons. Since the microstructures are similar in middle layer and free surface (Figs. 4), the pole figures in Figs. 5(c) and (d) could represent the whole ribbons. It is seen that the austenite has a strong fiber texture with the $<100>_A$//ND (the normal to ribbon plane), which is consistent with the typical texture of cubic metals formed during solidification, where the <100> direction of each crystal, or grain, is close to the heat transfer direction; the ND direction is the maximum cooling rate direction in the studied melt-spun ribbons [38, 64]. Moreover, as Fig. 5(d) shows, the martensite also exhibits a fiber type texture with the $<010>_M$ //ND, which should be attributed to the texture inheritance from the austenite through the specific orientation relationship between austenite and martensite [65].

With the determined crystal structure and microstructure information, the observation of a low thermal hysteresis in the presently studied ribbons can be discussed. As is known to us, the hysteresis loss is closely related to the stressed transition layer appearing at the interface regions between austenite and martensite during the structural transition, owing to the geometrical mismatch between both phases that gives rise to a barrier that should be overcome with the corresponding energy consumption [23, 28]. In theory, the geometrical compatibility between austenite and martensite can be quantitatively evaluated by the so-called cofactor conditions [28]. Ideal geometrical compatibility requires the middle eigenvalue λ_2 of the 3×3 '*transformation stretch matrix*' $\boldsymbol{U}$ and the norms X_I ($X_I = |\boldsymbol{U}^{-1}\hat{e}|$) and X_{II} ($X_{II} = |\boldsymbol{U}\hat{e}|$) for type-I and type-II twins equal to 1, where $\hat{e}$ is the unit vector aligned with the two-fold axes associated to these twins. With the determined lattice parameters of austenite and martensite, we found that λ_2=1.0014, X_I = 1.0104 and X_{II}= 0.9954 in the investigated ribbon. Note that these λ_2, X_I and X_{II} values are very close to 1, suggesting a good geometrical compatibility between the austenite and the martensite in the synthesized $Ni_{50}Mn_{35.25}In_{14.75}$ melt-spun ribbon. In the crystallographic theory of martensitic transformation [25, 63], the condition λ_2 = 1 denotes that a single martensite variant can form an invariant plane (*habit plane*) with austenite, which is in good agreement with our microstructural investigations (Fig. 5(b)).

It is well known that the microstructure of materials has also an important effect on the hysteresis [31-33]. The melt-spun ribbons studied in the present work show a grain-refined microstructure with an average grain size (initial austenite) of around 10 μm. This is about 10

times smaller than the one typically found in the bulk alloys (> 100 μm) [62]. As the grain boundary regions of initial austenite favor the nucleation of the new phase (Fig. 5(b)), the fine microstructure could be able to reduce the energy that the structural transition demands, thus reducing the hystereses loss. A similar grain size effect on hystereses was also observed in Gd_5Ge_4 alloy [33]. Moreover, theoretically, the texture of materials might be also linked to the hysteresis behavior. As can be seen in the dashed box in Fig. 5(a), the martensite plates within the adjacent austenite grains stretch in close directions, which is generally observed in highly-textured NiMn-based alloys [40, 66]. With respect to the strain accommodation of martensitic transformation in the vicinity of grain boundary [25, 63], the lattice distortion induced by the structural transition should be more easily accommodated in neighboring grains with a similar orientation than in those with random orientations. Thus, the strong texture of the studied ribbons might be favorable to reduce the hystereses loss. Besides, recently, it is reported that the thin thickness of ribbon samples has also a positive effect to narrow the thermal hysteresis in $Ni_{43}Mn_{46}Sn_{11}$ alloy [32].

4. **CONCLUSIONS**

In summary, the crystallographic and microstructural studies carried out on $Ni_{50}Mn_{35.25}In_{14.75}$ ribbons fabricated by conventional melt-spinning technique exhibiting a moderate maximum value of the magnetic entropy change (11 $J \cdot kg^{-1} \cdot K^{-1}$ at 5 T), and a low thermal (6 K) and magnetic field induced hysteresis (0.73 $J \cdot kg^{-1}$ at 2 T), showed that: a) the austenite and martensite phases have a cubic $L2_1$ and monoclinic incommensurate 6M modulated structure (superspace group of *I2/m*(*α*0*γ*)*00*), respectively); b) the ribbons exhibit a fine microstructure with an average grain size of the initial austenite phase of around 10 μm and a strong fiber texture of both austenite and martensite, (*i.e.* $<100>_A$//ND and $<010>_M$ //ND); c) during the inverse martensitic transformation, the austenite primarily forms at the initial austenite grain boundaries; and d) a good geometrical compatibility between austenite and martensite is confirmed based on the cofactor conditions analyses. Thus, the low thermal hysteresis and reduced resistance to the magnetostructural transformation observed in the studied melt-spun ribbons should result from the favorable combination of these aforementioned factors.

ACKNOWLEDGEMENTS

This work is supported by the National Natural Science Foundation of China (Grant No. 51431005, 51571056, 51771048, 51771044, 51601033), Laboratorio Nacional de Investigaciones en Nanociencias y Nanotecnología (LINAN, IPICYT), the Fundamental Research Funds for the Central Universities (Grant No. N170203009), the 111 Program of China (Grant No. B07015), and the French State through the Program "Investment in the future" operated by the National Research Agency and referenced by ANR-11-LABX-0008-01 (LabEx DAMAS). J.L. Sánchez Llamazares acknowledges the support received from Laboratorio Nacional de Investigaciones en Nanociencias y Nanotecnología (LINAN, IPICyT). C.F. Sánchez-Valdés is grateful to DMCU-UACJ for supporting his research work through PFCE and academic mobility grants; the financial support received from CONACYT and PRODEP-SEP, Mexico, is also acknowledged.

REFERENCES

[1] T. Krenke, E. Duman, M. Acet, E.F. Wassermann, X. Moya, L. Manosa, A. Planes, Inverse magnetocaloric effect in ferromagnetic Ni−Mn−Sn alloys, Nat. Mater. 4 (2005) 450-454.
[2] R. Kainuma, Y. Imano, W. Ito, Y. Sutou, H. Morito, S. Okamoto, O. Kitakami, K. Oikawa, A. Fujita, T. Kanomata, K. Ishida, Magnetic-field-induced shape recovery by reverse phase transformation, Nature 439 (2006) 957-960.
[3] B. Hernando, J.L.S. Llamazares, J.D. Santos, M.L. Sanchez, L. Escoda, J.J. Sunol, R. Varga, C. Garcia, J. Gonzalez, Grain oriented NiMnSn and NiMnIn Heusler alloys ribbons produced by melt spinning: Martensitic transformation and magnetic properties, J. Magn. Magn. Mater. 321 (2009) 763-768.
[4] X.G. Zhao, C.C. Hsieh, W.C. Chang, W. Liu, Z.D. Zhang, Effects of Si substitution on phase transformation and exchange bias in Ni−Mn−In ribbons, J. Phys. Conf. Ser. 266 (2011) 012128.
[5] J.L. Sánchez Llamazares, H. Flores-Zuniga, C. Sanchez-Valdes, C.A. Ross, C. Garcia, Refrigerant capacity of austenite in as-quenched and annealed $Ni_{51.1}Mn_{31.2}In_{17.7}$ melt spun ribbons, J. Appl. Phys. 111 (2012) 07A932.
[6] J. Liu, T. Gottschall, K.P. Skokov, J.D. Moore, O. Gutfleisch, Giant magnetocaloric effect driven by structural transitions, Nat. Mater. 11 (2012) 620-626.
[7] J.I. Perez-Landazabal, V. Recarte, V. Sanchez-Alarcos, S. Kustov, D. Salas, E. Cesari, Effect of magnetic field on the isothermal transformation of a Ni−Mn−In−Co magnetic shape memory alloy, Intermetallics 28 (2012) 144-148.
[8] L. Gonzalez-Legarreta, T. Sanchez, W.O. Rosa, J. Garcia, D. Serantes, R. Caballero-Flores, V.M. Prida, L. Escoda, J.J. Sunol, V. Koledov, B. Hernando, Annealing influence on the microstructure and magnetic properties of Ni−Mn−In alloys ribbons, J. Supercond. Novel. Magn. 25 (2012) 2431-2436.

[9] L. Gonzalez-Legarreta, D. Gonzalez-Alonso, W.O. Rosa, R. Caballero-Flores, J.J. Sunol, J. Gonzalez, B. Hernando, Magnetostructural phase transition in off-stoichiometric Ni−Mn−In Heusler alloy ribbons with low In content, J. Magn. Magn. Mater. 383 (2015) 190-195.
[10] D.M. Liu, D.Y. Cong, X.M. Sun, H.Y. Chen, Z.H. Nie, Z. Chen, Y. Zhang, C. Zhu, Y.H. Qu, J. Zhu, Y.D. Wang, Low-hysteresis tensile superelasticity in a Ni−Co−Mn−Sn magnetic shape memory microwire, J. Alloy Compd. 728 (2017) 655-658.
[11] Z. Yang, D.Y. Cong, X.M. Sun, Z.H. Nie, Y.D. Wang, Enhanced cyclability of elastocaloric effect in boron-microalloyed Ni−Mn−In magnetic shape memory alloys, Acta Mater. 127 (2017) 33-42.
[12] W. Maziarz, A. Wojcik, J. Grzegorek, A. Zywczak, P. Czaja, M.J. Szczerba, J. Dutkiewicz, E. Cesari, Microstructure, magneto-structural transformations and mechanical properties of $Ni_{50}Mn_{37.5}Sn_{12.5-x}In_x$ (x=0, 2, 4, 6% at.) metamagnetic shape memory alloys sintered by vacuum hot pressing, J. Alloy Compd. 715 (2017) 445-453.
[13] R. Chulist, L. Straka, A. Sozinov, T. Tokarski, W. Skrotzki, Branched needle microstructure in Ni−Mn−Ga 10M martensite: EBSD study, Acta Mater. 128 (2017) 113-119.
[14] S. Pandey, A. Quetz, P.J. Ibarra-Gaytan, C.F. Sanchez-Valdes, A. Aryal, I. Dubenko, D. Mazumdar, J.L.S. Llamazares, S. Stadler, N. Ali, Effects of annealing on the magnetic properties and magnetocaloric effects of B doped Ni−Mn−In melt-spun ribbons, J. Alloy Compd. 731 (2018) 678-684.
[15] A.M. Tishin, Magnetocaloric effect in the vicinity of phase transitions, in: K.H.J. Buschow (Ed.), Handbook of magnetic materials, vol. 12, Elsevier, Amsterdam, 1999, pp. 395-524.
[16] V. Franco, J.S. Blazquez, B. Ingale, A. Conde, The magnetocaloric effect and magnetic refrigeration near room temperature: Materials and models, Annu. Rev. Mater. Res. 42 (2012) 305-342.
[17] P. Lázpita, J.M. Barandiarán, J. Gutiérrez, C. Mondelli, A. Sozinov, V.A. Chernenko, Polarized neutron study of Ni−Mn−Ga alloys: Site-specific spin density affected by martensitic transformation, Phys. Rev. Lett. 119 (2017) 155701.
[18] P. Lázpita, M. Sasmaz, E. Cesari, J.M. Barandiarán, J. Gutiérrez, V.A. Chernenko, Martensitic transformation and magnetic field induced effects in $Ni_{42}Co_8Mn_{39}Sn_{11}$ metamagnetic shape memory alloy, Acta Mater. 109 (2016) 170-176.
[19] P. Czaja, W. Maziarz, J. Przewoznik, A. Zywczak, P. Ozga, M. Bramowicz, S. Kulesza, J. Dutkiewicz, Surface topography, microstructure and magnetic domains in Al for Sn substituted metamagnetic Ni-Mn-Sn Heusler alloy ribbons, Intermetallics 55 (2014) 1-8.
[20] Z.B. Li, Z.Z. Li, B. Yang, Y.D. Zhang, C. Esling, X. Zhao, L. Zuo, Large low-field magnetocaloric effect in a directionally solidified $Ni_{50}Mn_{18}Cu_7Cu_{25}$ alloy, Intermetallics 88 (2017) 31-35.
[21] A. Wojcik, W. Maziarz, M.J. Szczerba, M. Sikora, A. Ywczak, C.O. Aguilar-Ortiz, P. Alvarez-Alonso, E. Villa, H. Flores-Zuniga, E. Cesari, J. Dutkiewicz, V.A. Chernenko, Transformation behavior and inverse caloric effects in magnetic shape memory $Ni_{44-x}Cu_xCo_6Mn_{39}Sn_{11}$ ribbons, J. Alloy Compd. 721 (2017) 172-181.
[22] X.L. Wang, F. Sun, J.M. Wang, Q. Yu, Y.Y. Wu, H. Hua, C.B. Jiang, Influence of annealing temperatures on the magnetostructural transition and magnetocaloric effect of $Ni_{40}Co_{10}Mn_{40}Sn_{10}$ powders, J. Alloy Compd. 691 (2017) 215-219.
[23] Y.T. Song, X. Chen, V. Dabade, T.W. Shield, R.D. James, Enhanced reversibility and unusual microstructure of a phase-transforming material, Nature 502 (2013) 85-88.

[24] M. Brokate, Hysteresis and phase transitions, Springer-Verlag, New York, 1996.
[25] K. Bhattacharya, Microstructure of martensite: Why it forms and how it gives rise to the shape-memory effect, Oxford University Press, Oxford, 2003.
[26] V.K. Pecharsky, K.A. Gschneidner Jr., Y. Mudryk, D. Paudyal, Making the most of the magnetic and lattice entropy changes, J. Magn. Magn. Mater. 321 (2009) 3541-3547.
[27] D.V. Ragone, Thermodynamics of materials, Wiley, New York, 1995.
[28] Z.Y. Zhang, R.D. James, S. Müller, Energy barriers and hysteresis in martensitic phase transformations, Acta Mater. 57 (2009) 4332-4352.
[29] E. Stern-Taulats, P.O. Castillo-Villa, L. Mañosa, C. Frontera, S. Pramanick, S. Majumdar, A. Planes, Magnetocaloric effect in the low hysteresis Ni−Mn−In metamagnetic shape-memory Heusler alloy, J. Appl. Phys. 115 (2014) 173907.
[30] V. Srivastava, X. Chen, R.D. James, Hysteresis and unusual magnetic properties in the singular Heusler alloy $Ni_{45}Co_5Mn_{40}Sn_{10}$, Appl. Phys. Lett. 97 (2010) 014101.
[31] O. Gutfleisch, T. Gottschall, M. Fries, D. Benke, I. Radulov, K.P. Skokov, H. Wende, M. Gruner, M. Acet, P. Entel, M. Farle, Mastering hysteresis in magnetocaloric materials, Phil. Trans. R. Soc. A 374 (2016) 20150308.
[32] Y. Zhang, Q. Zheng, W. Xia, J. Zhang, J. Du, A. Yan, Enhanced large magnetic entropy change and adiabatic temperature change of $Ni_{43}Mn_{46}Sn_{11}$ alloys by a rapid solidification method, Scripta Mater. 104 (2015) 41-44.
[33] J.D. Moore, G.K. Perkins, Y. Bugoslavsky, M.K. Chattopadhyay, S. Roy, P. Chaddah, V.K. Pecharsky, K.A. Gschneidner Jr., L. Cohen, Reducing the operational magnetic field in the prototype magnetocaloric system Gd_5Ge_4 by approaching the single cluster size limit, Appl. Phys. Lett. 88 (2006) 072501.
[34] T. Gottschall, E. Stern-Taulats, L. Manosa, A. Planes, K.P. Skokov, O. Gutfleisch, Reversibility of minor hysteresis loops in magnetocaloric Heusler alloys, Appl. Phys. Lett. 110 (2017) 4.
[35] T. Gottschall, K.P. Skokov, B. Frincu, O. Gutfleisch, Large reversible magnetocaloric effect in Ni−Mn−In−Co, Appl. Phys. Lett. 106 (2015) 021901.
[36] J.D. Santos, T. Sanchez, P. Alvarez, M.L. Sanchez, J.L. Sánchez Llamazares, B. Hernando, L. Escoda, J.J. Suñol, R. Varga, Microstructure and magnetic properties of $Ni_{50}Mn_{37}Sn_{13}$ Heusler alloy ribbons, J. Appl. Phys. 103 (2008) 07B326.
[37] J.L. Sánchez Llamazares, B. Hernando, C. García, J. González, L. Escoda, J.J. Suñol, Martensitic transformation in $Ni_{50.4}Mn_{34.9}In_{14.7}$ melt spun ribbons, J. Phys. D: Appl. Phys. 42 (2009) 045002.
[38] Z. Li, J. Wang, Y. Zhang, K. He, X. Zhao, L. Zuo, G. Hofer, C. Esling, Texturation of Ni−Co−Mn−In Ribbons by Melt Spinning, Adv. Eng. Mater. 12 (2010) 1024-1028.
[39] X.G. Zhao, C.C. Hsieh, J.H. Lai, X.J. Cheng, W.C. Chang, W.B. Cui, W. Liu, Z.D. Zhang, Effects of annealing on the magnetic entropy change and exchange bias behavior in melt-spun Ni−Mn−In ribbons, Scripta Mater. 63 (2010) 250-253.
[40] Z.B. Li, J.L. Sánchez Llamazares, C.F. Sánchez-Valdés, Y.D. Zhang, C. Esling, X. Zhao, L. Zuo, Microstructure and magnetocaloric effect of melt-spun $Ni_{52}Mn_{26}Ga_{22}$ ribbon, Appl. Phys. Lett. 100 (2012) 174102.
[41] Z.B. Li, B. Yang, N.F. Zou, Y.D. Zhang, C. Esling, W.M. Gan, X. Zhao, L. Zuo, Crystallographic characterization on polycrystalline Ni−Mn−Ga alloys with strong preferred orientation, Materials 10 (2017) 20.

[42] F. Bachmann, R. Hielscher, H. Schaeben, Texture Analysis with MTEX – Free and Open Source Software Toolbox, Solid State Phenom. 160 (2010) 63-68.
[43] Y.B. Yang, X.B. Ma, X.G. Chen, J.Z. Wei, R. Wu, J.Z. Han, H.L. Du, C.S. Wang, S.Q. Liu, Y.C. Yang, Y. Zhang, J.B. Yang, Structure and exchange bias of $Ni_{50}Mn_{37}Sn_{13}$ ribbons, J. Appl. Phys. 111 (2012) 07A916.
[44] J. Sharma, K. Suresh, Observation of large exchange bias effect in bulk $Mn_{50}Ni_{41}Sn_9$ Heusler alloy, IEEE Trans. Magn. 50 (2014) 1-4.
[45] K. Prusik, E. Matyja, M. Kubisztal, M. Zubko, R. Swadzb, Magnetic properties and structure of the Ni−Co−Mn−In alloys with the boron addition, Acta Phys. Pol. A 131 (2017) 1240-1243.
[46] J.L. Sánchez Llamazares, B. Hernando, V.M. Prida, C. Garcia, J. Gonzalez, R. Varga, C.A. Ross, Magnetic field influence on the structural transformation in ferromagnetic shape memory alloy $Mn_{50}Ni_{40}In_{10}$ melt spun ribbons, J. Appl. Phys. 105 (2009).
[47] H.L. Yan, C.F. Sanchez-Valdes, Y.D. Zhang, J.L. Sánchez Llamazares, Z.B. Li, B. Yang, C. Esling, X. Zhao, L. Zuo, Crystallographic charaterisitics and magnetcocaloric effect of Ni−Co−Mn−In ribbon (preparation), (2017).
[48] T. Gottschall, K.P. Skokov, D. Benke, M.E. Gruner, O. Gutfleisch, Contradictory role of the magnetic contribution in inverse magnetocaloric Heusler materials, Phys. Rev. B 93 (2016) 184431.
[49] A.S.B. Madiligama, P. Ari-Gur, Y. Ren, V.V. Koledov, E.T. Dilmieva, A.P. Kamantsev, A.V. Mashirov, V.G. Shavrov, L. Gonzalez-Legarreta, B.H. Grande, Thermal and magnetic hysteresis associated with martensitic and magnetic phase transformations in $Ni_{52}Mn_{25}In_{16}Co_7$ Heusler alloy, J. Magn. Magn. Mater. 442 (2017) 25-35.
[50] B. Banerjee, On a generalised approach to first and second order magnetic transitions, Phys. Lett. 12 (1964) 16-17.
[51] A.M. Tishin, Y.I. Spichkin, The magnetocaloric effect and its applications, CRC Press, Bristol, 2003.
[52] X.C. Zhong, J.X. Min, Z.G. Zheng, Z.W. Liu, D.C. Zeng, Critical behavior and magnetocaloric effect of $Gd_{65}Mn_{35-x}Ge_x$ (x = 0, 5, and 10) melt-spun ribbons, J. Appl. Phys. 112 (2012) 033903.
[53] A. Yan, K.H. Müller, O. Gutfleisch, Magnetocaloric effect in $LaFe_{11.8-x}Co_xSi_{1.2}$ melt-spun ribbons, J. Alloy Compd. 450 (2008) 18-21.
[54] K.A. Gschneidner Jr., V.K. Pecharsky, A.O. Tsokol, Recent developments in magnetocaloric materials, Rep. Prog. Phys. 68 (2005) 1479-1539.
[55] N.F. Zou, Z.B. Li, Y.D. Zhang, C.F. Sanchez-Valdes, J.L. Sánchez Llamazares, C. Esling, B. Yang, X. Zhao, L. Zuo, Transformation process dependent magnetocaloric properties of annealed $Ni_{50}Mn_{18}Cu_7Ga_{25}$ ribbons, J. Alloy Compd. 698 (2017) 731-738.
[56] H.L. Yan, Y.D. Zhang, N. Xu, A. Senyshyn, H.-G. Brokmeier, C. Esling, X. Zhao, L. Zuo, Crystal structure determination of incommensurate modulated martensite in Ni−Mn−In Heusler alloys, Acta Mater. 88 (2015) 375-388.
[57] T. Krenke, M. Acet, E.F. Wassermann, X. Moya, L. Mañosa, A. Planes, Ferromagnetism in the austenitic and martensitic states of Ni−Mn−In alloys, Phys. Rev. B 73 (2006) 174413.
[58] A. Le Bail, H. Duroy, J.L. Fourquet, Ab-initio structure determination of $LiSbWO_6$ by X-ray powder diffraction, Mater. Res. Bull. 23 (1988) 447-452.
[59] S. Van Smaalen, Incommensurate crystallography, Oxford University Press, Oxford, 2007.

[60] P. Devi, S. Singh, K. Manna, E. Suard, V. Petricek, C. Felser, D. Pandey, Adaptive modulation in $Ni_2Mn_{1.4}In_{0.6}$ magnetic shape memory Heusler alloy, arXiv (2016) 1611.06688.
[61] H.L. Yan, C.Y. Zhang, Y.D. Zhang, X.L. Wang, C. Esling, X. Zhao, L. Zuo, Crystallographic insights into Ni−Co−Mn−In metamagnetic shape memory alloys, J. Appl. Cryst. 49 (2016) 1585-1592.
[62] H.L. Yan, B. Yang, Y.D. Zhang, Z.B. Li, C. Esling, X. Zhao, L. Zuo, Variant organization and mechanical detwinning of modulated martensite in Ni−Mn−In metamagnetic shape-memory alloys, Acta Mater. 111 (2016) 75-84.
[63] C.M. Wayman, Introduction to the crystallography of martensitic transformations, Macmillan, New York, 1964.
[64] D.M. Stefanescu, Science and engineering of casting solidification, Springer-Verlag, New York, 2009.
[65] Z.B. Li, Y.W. Jiang, Z.Z. Li, Y.Q. Yang, B. Yang, Y.D. Zhang, C. Esling, X. Zhao, L. Zuo, Texture inheritance from austenite to 7 M martensite in Ni−Mn−Ga melt-spun ribbons, Results Phys. 6 (2016) 428-433.
[66] J. Liu, T.G. Woodcock, N. Scheerbaum, O. Gutfleisch, Influence of annealing on magnetic field-induced structural transformation and magnetocaloric effect in Ni−Mn−In−Co ribbons, Acta Mater. 57 (2009) 4911-4920.

1. Textured $Ni_{50}Mn_{35.25}In_{14.75}$ ribbons with low hysteresis were fabricated.

2. Martensite with 6M structure has a self-accommodated microstructure.

3. Lattices of austenite and martensite have a good geometrical compatibility.

4. Origin of low hysteresis was discussed based on crystal structure and microstructure.